Publishing Excellence Inspiring Progress
ARISTON PUBLICATIONS
MatSci Express
ISSN: 2997-8440 www.aristonpubs.com/matsci-express https://doi.org/10.69626/mse.2024.0105

RESEARCH ARTICLE

Investigating the Potential of Gd^{3+} doped $LiBPO_4$ Phosphors in Improving White Lighting Applications: Synthesis, Characterization, and Analysis of Their Optical Properties

Aasim Rashid Khanday [1], Showket Ahmad Bhat [1, *], Faheem Ahmad Dar [2], Mohd. Ikram [1]

ABSTRACT: This study investigates the impact of Gd^{3+} doping on the structural and optical characteristics of $LiBaPO_4$. In this study, the solid-state reaction route was utilized to synthesized $LiBa_{1-x}Gd_xPO_4$ compounds with varying compositions (x = 0, 0.04, and 0.08). In this study, the phase of the samples was determined through Rietveld refinement analysis using Foolproof software. This analysis allowed us to obtain refined parameters such as lattice constants, volume of the unit cell, and goodness of fit (χ^2). The samples were observed to exhibit crystallization in the trigonal phase, characterized by the space group P31c. In this study, the surface morphology of the sample was analyzed using field emission scanning electron microscopy (FESEM). The obtained FESEM images were further processed using ImageJ software to calculate the grain size. In this study, the optical band gap was determined through the application of the tauc plot method. The results revealed a decreasing trend in the band gap values (ranging from 3.06 eV to 2.14 eV) as the dopant concentration was increased. This study investigates the photoluminescence properties of brilliant red luminescent phosphor spheres and their potential application in red luminescent optical devices. The results indicate that these phosphor spheres exhibit strong red luminescence, indicating their suitability for use in such devices.

Keywords: $LiBPO_4$ Phosphor, White Light, Rietveld Refinement, Trigonal Phase, Tauc Plot, Luminescent

Received: 08 February 2024; Revised: 27 March 2024; Accepted: 19 April 2024; Published Online: 01 June 2024

1. INTRODUCTION

Considerable research attention has been directed towards optical materials with the aim of advancing the development of materials suitable for applications in white lighting [1, 2]**.** Phosphor-converted white LEDs, commonly referred to as PC-WLEDs, are a type of light-emitting diode that harnesses the phenomenon of phosphorescence to produce white light. These LEDs employ a blue-emitting indium gallium nitride (InGaN) chip as the primary light source. To achieve the desired white light output, the InGaN chip is coated with a layer of Ce^{+3} doped Yttrium aluminum garnet, a mineral that emits yellow light when excited. This combination of blue and yellow light emissions results in the perception of white light. The utilization of phosphorus as a means to replicate white light is a well-established practice in various scientific and technological domain s. This method's light has a number of limitations, including an unfavorably high correlated color temperature (CCT) of 4500 K, decreased color purity, and a poor color rendering index (CRI) of between 70 and 80. Certain limitations arise as a consequence of the light's absence of a red component [2]. An innovative strategy was used that made use of a trio of primary color-emitting phosphors in order to get around the current constraints. These phosphors were chosen with care to have the special ability to be excited by an easily available, n-UV or blue-emitting LED chip that is marketed. This new

[1] Solid State Laboratory, Department of Physics, National Institute of Technology (NIT), Srinagar, Jammu and Kashmir 190006, India
[2] Solid State Research Laboratory, Department of Physics, University of Kashmir, Srinagar, Jammu and Kashmir 190006, India.

* Author to whom correspondence should be addressed: showketbht7@gmail.com (Showket Ahmad Bhat)

method's ultimate goal was to produce white light in order to get over the limitations outlined above [3]. According to the scientific literature now in use, it has been found that a sizeable fraction of phosphors that are widely available on the commercial market and capable of generating red light are mostly made of rare earth-doped nitrides. Some notable instances include $Sr_2Si_5N_8$:Eu^{+2} and $CaAlSiN_3$:Eu^{+3} [4]. The elevated response temperature, coupled with the utilization of nitrogen air, contributes to an escalation in production costs and enhances the breaking point for subsequent commercialization endeavors [5]. Moreover, it has been observed that the nitride-based red phosphors exhibit a wide emission spectrum spanning from the orange to red region of the electromagnetic spectrum. This characteristic leads to a significant dissipation of energy within the near-infrared range. In light of the aforementioned, it is of utmost importance to undertake a thorough investigation into phosphors exhibiting robust red emission within the visible spectrum, while also possessing the ability to effectively absorb ultraviolet (UV) radiation. In light of the aforementioned, it is of utmost importance to undertake a thorough investigation into phosphors exhibiting robust red emission within the visible spectrum, while concurrently possessing the ability to effectively absorb ultraviolet (UV) radiation. In accordance with prevailing scientific understanding, it is widely acknowledged that phosphors, as a general class of materials, consist of a composite structure comprising two distinct units. The initial candidate exhibits characteristics that render it a viable host. The successful incorporation of an activator within the crystal lattice necessitates the presence of a suitable host matrix. Ternary orthophosphates, denoted as $ABPO_4$, have successfully undergone synthesis, wherein A represents a range of alkali earth metals including Li, Na, K, Rb, and Cs, while B encompasses alkaline earth metals such as Mg, Ca, Sr, and Ba. Ternary orthophosphates, denoted as $ABPO_4$, have been successfully synthesized using a range of alkali earth metals (A = Li, Na, K, Rb, Cs) and alkaline earth metals (B = Mg, Ca, Sr, Ba). The object under scrutiny has garnered significant interest owing to its exceptional characteristics, including superior quality, remarkable chemical and thermal stability, an outstanding threshold for optical damage, a wide band gap, and a heightened capacity for PO_4 absorption within the ultraviolet spectrum [6]**.**

In addition to the aforementioned characteristics, it is noteworthy that phosphates exhibit an intriguing attribute in the form of intermediate phonon energy, typically ranging from 1000 to 1200 cm^{-1}. By significantly reducing the incidence of non-radiative transitions within the matrix, this specific property plays a critical role in reducing heat production inside the host material. Numerous uses of oxide-based host materials may be identified in the field of advanced technology. The utilization of activators renders the host material highly appealing for the incorporation of phosphors [7]. Oxide-based host materials have found numerous applications in the realm of advanced technology. Among these applications, superconductors, supercapacitors, radio frequency devices, and microwaves stand out as prominent examples. These materials have demonstrated exceptional properties and have proven to be invaluable in various scientific and engineering endeavors. In the realm of technological advancements, various applications have emerged that showcase the prowess of electronic components, non-contact optical thermometry, and solid-state lighting. These remarkable innovations have revolutionized numerous industries and continue to push the boundaries of scientific exploration. Due to their complex circuitry and capacity to alter electrical impulses, electronic components have become fundamental to contemporary civilization. From microprocessors that power our computers to transistors that amplify signals in communication devices, these components have paved the way for unprecedented advancements in information technology, telecommunications, and automation. [8-12]. The inclusion of an activator is a crucial element in the composition of phosphor. The presence of activator ions within the interstitial or lattice space of the host matrix has been observed. The intriguing properties of rare earth have captured the attention of material scientists, sparking a keen interest in further exploration and investigation. The meticulous examination of these entities, owing to their distinct 4f–4f transitions, renders them a highly auspicious activator. The utilization of Eu^{+3} ions in display and lighting applications is facilitated by their distinctive deep reddish emission. However, the practical implementation of Eu^{+3} is hindered by its significant economic cost, posing a substantial obstacle to its widespread utility in these domains.

The compound known as orthophosphate phosphorous, denoted by the chemical formula $ABPO_4$, is of particular interest in scientific research. It is worth noting that in this formula, the letter A represents a monovalent cation, while the letter B represents a divalent cation. This compound has garnered attention due to its unique properties and potential applications in various fields. The subject of interest under investigation exhibits intriguing characteristics due to its remarkable optical properties. Additionally, it demonstrates commendable thermal and hydrolytic stability, further enhancing its scientific significance. The investigation of the optical characteristics of the $ABPO_4$ phosphor, a phosphate-based compound, has garnered significant attention from numerous researchers thus far. Numerous scientific investigations have been conducted thus far, wherein a multitude of diligent researchers have successfully synthesized phosphors based on phosphates, specifically of the $ABPO_4$ variety. A comprehensive investigation has been conducted on a range of orthophosphates doped with Eu^{3+} ions. The studied compounds encompass $LiMgPO_4$, $LiSrPO_4$, $LiBaPO_4$, $NaBaPO_4$, $KBaPO_4$, and $KSrPO_4$. These materials have been extensively characterized and their properties elucidated [13-18]. To date, no reports have been documented regarding the utilization of Gd^{3+} doped $LIBaPO_4$ phosphors in the field of photoluminescence. In the present investigation, the synthesis of $LiBaPO_4$ was accomplished with notable success. Furthermore, the synthesized material was subjected to doping with varying quantities of Gd^{3+}.

2. EXPERIMENTAL DETAILS

The experimentation was carried out by the general Solid State Reaction Method, the precursors used to synthesize $LiBaPO_4$ and Gd^{3+} doped $LiBaPO_4$ ($LiBa_{1-x}Gd_xPO_4$) are sigma Aldrich grade Li_2CO_3(99.9%), $BaCO_3$(99.9%),NH_4PO_4(99.9%) and Gd_2O_3(99.9%).

To synthesize $LiBaPO_4$ and $LiBa_{1-x}Gd_xPO_4$,the precursors Li_2CO_3,$BaCO_3$,NH_4PO_4 and Gd_2O_3 are used in appropriate stoichiometric ratios by weight and acetone was used as solvent. These precursors were weighed and then grinded using motor pestle for 3 hours to get a homogeneous mixture. These samples were calcined 600 ºC for 6 hours with heating rate of 5 ºC/min and cooling naturally. These heated samples are now again grinded using motor pestle for 4 hours to get the homogenous mixture of the desired samples. Final heating(sintering) was done at 1100ºC for 12 hours with the same heating rate and cooling as above mentioned .These heating's were done to remove the impurity and make these precursors to react well to form desired $LiBaPO_4$ and $LiBa_{1-x}Gd_xPO_4$ (X=0.04,0.08). The XRD was done for phase confirmation, the phases were confirmed successfully with trigonal structure and space group P31c.

The characterization was done by several techniques including X-Ray Diffraction (XRD) by Rigaku X-ray diffractometer for phase confirmation, Field Emission Scanning Electron Microscope (FE-SEM) by JEOL JSM600F for surface morphology, Ultra-Violet Visible spectroscopy by Shimadzu UV-Vis-NIR spectrophotometer for optical bandgap, Fourier Transform Infrared Spectra (FTIR) by Perkin Elmer Spectrum Two for nature of bonds, and Photoluminescence Spectra (PL) by Cary Eclipse Spectrophotometer used to determine the M^{3+} (M=Eu,Gd and Dy etc.) ion's valance status.

3. RESULTS AND DISCUSSION

3.1. Crystal properties

The purity of the phase and the crystalline nature of $LiBa_{1-x}Gd_xPO_4$ (X=0.00, 0.04, 0.06, 0.08) were analyzed using XRD patterns that are shown in Fig. 1. On comparing with the literature, it was found that the phase of the samples is trigonal with the space group P31c [1]**.** Peak intensities are seen to increase when doping concentration is increased from 0 to 0.08. This shows the improvement in the crystallinity [19]**.** Scherrer formula was used to calculate the crystalline size and it was was found to be 43, 47 and 65 nm for the samples with doping concentrations (x) 0, 0.04 and 0.08 respectively. A shift was observed in the position of peaks on doping the pure sample of $LiBaPO_4$ with Gd^{3+} ions, attributed to different ionic radii of the host and guest site ions.

The confirmation of the phase of the samples is achieved through the utilization of the Rietveld refinement technique, as depicted in Fig. 2. The refined parameters obtained through the process of Rietveld refinement have been meticulously organized and presented in Table 1. The table presents the goodness of fit (GOF) values for $LiBaPO_4$, $LiBa_{0.96}Gd_{0.04}PO_4$, and $LiBa_{0.92}Gd_{0.08}PO_4$, which are 2.41, 2.34, and 2.19, respectively. The obtained value of the Goodness of Fit (GOF) metric, approximately equal to 1, indicates an exceptional level of agreement between the observed data and the model. This result provides strong evidence that the estimated parameters have been accurately determined [20].

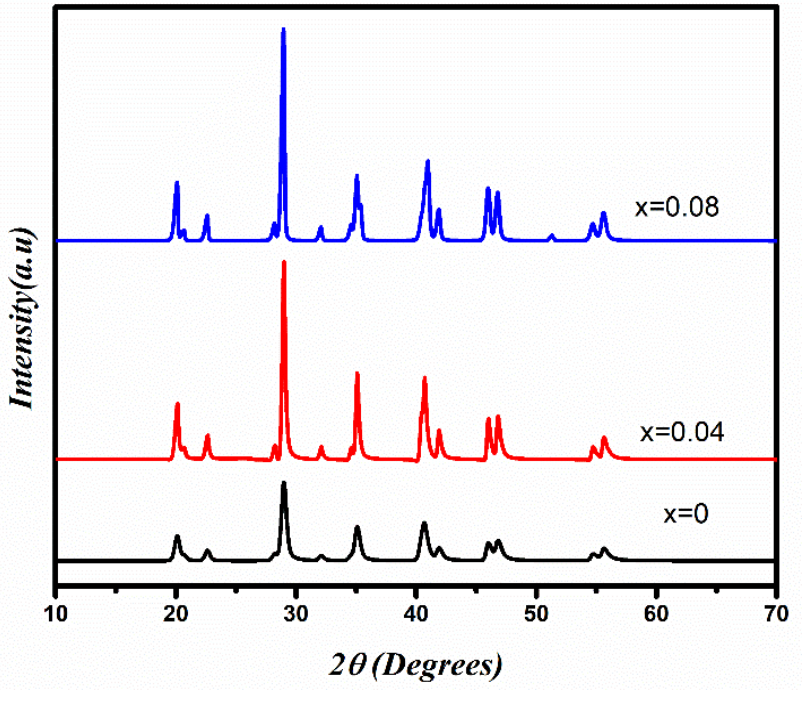

Fig. 1. XRD Patterns of $LiBa_{(1-x)}PO_4$: xGd^{3+}.

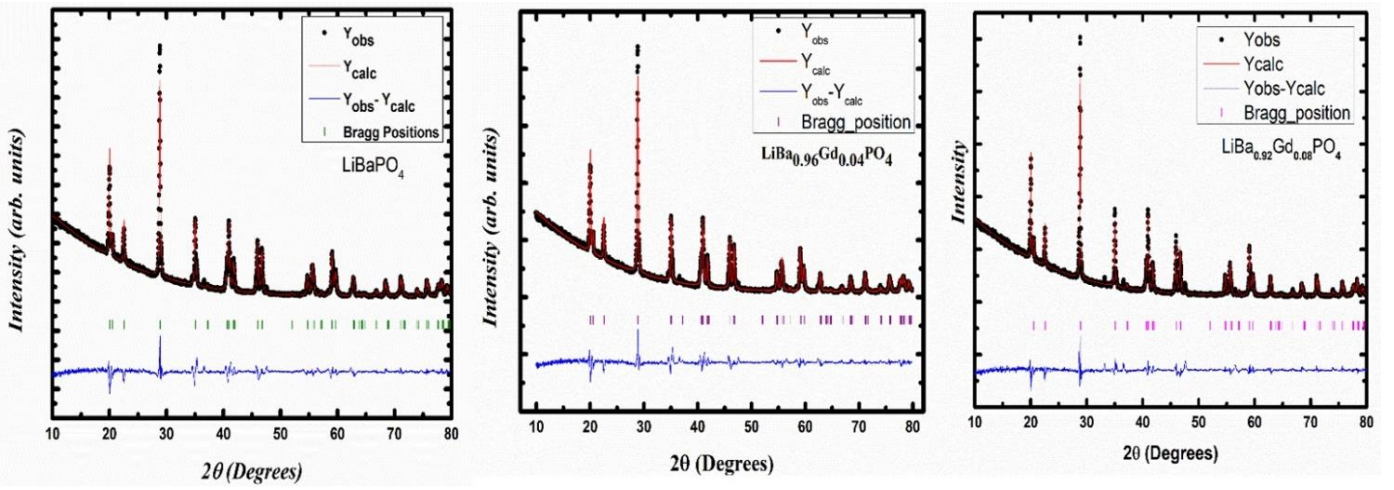

Fig. 2. Rietveld refinement plots of $LiBa_{(1-x)}Gd_xPO_4$; X= 0, 0.04, and 0.08.

Table 1. Rietveld refinement parameters of $LiBa_{(1-x)}Gd_xPO_4$; x= 0, 0.04, and 0.08.

Parameters	x = 0	x = 0.04	x = 0.08
Crystal structure	Trigonal	Trigonal	Trigonal
Space-group	P31c	P31c	P31c
Lattice Parameters	a=b=5.12258 c=8.64338 α=β=90 γ=120	a=b=5.1227 c=8.6436 α=β=90 γ=120	a=b=5.1216 c=8.6445 α=β=90 γ=120
Unit Cell Volume (Å)	196.4195	196.4388	196.3759
Crystal Size (nm)	43	47	65
R_{wp}	8.19	7.97	7.30
R_{ex}	3.40	3.40	4.83
GOF(χ2)	2.41	2.34	2.19

The unit cell parameters exhibit slight modifications as a consequence of the disparity in the ionic radii between Gd^{3+} and Ba^{2+} ions. The formation of the three-dimensional network structure in $LiBaPO_4$ can be attributed to the presence of $[PO_4]$ and $[LiO_4]$ tetrahedrons. Within the intricate three-dimensional lattice, the Ba^{2+} ions are also strategically positioned. [21]. In the process of Gd^{3+} ion substitution for Ba^{2+} ions, a notable challenge arises in maintaining charge equilibrium within the host system. This predicament stems from the contrasting valence states exhibited by the Gd^{3+} and Ba^{2+} ions. In order to preserve their charge equilibrium, Gd^{3+} ions exhibit a propensity to form pairs. The formation of these pairs is initiated through the entrapment of an interstitial O^{2-} ion, which subsequently proceeds to occupy a specific region within the Ba^{2+} ion site [22].

3.2. Morphological properties

The investigation of the surface morphology of $LiBa_{1-x}Gd_xPO_4$ (where x = 0, 0.04, and 0.08) was conducted through the utilization of a Field Emission Scanning Electron Microscope (FESEM). Fig. 3 displays the Field Emission Scanning Electron Microscopy (FESEM) images along with their respective histograms. The grain size of the samples, namely $LiBaPO_4$, $LiBa_{0.96}Gd_{0.04}PO_4$, and $LiBa_{0.92}Gd_{0.08}PO_4$, was determined through the utilization of the ImageJ software. The calculated grain sizes were found to be 7.92 µm, 2.97 µm, and 2.74 µm, respectively. The experimental results reveal a direct correlation between the concentration

of Gd^{3+} ions and the observed porosity, as evidenced by the Field Emission Scanning Electron Microscopy (FESEM) images. This phenomenon suggests that the introduction of Gd^{3+} ions lead to an increase in porosity within the phosphor material. The porous network formed by the Gd^{3+} ions effectively hinders particle aggregation, resulting in the production of a phosphor material with a significantly enlarged surface area [23].

3.3. Fourier transform infrared spectroscopic studies

The Fourier Transform Infrared (FTIR) spectra of the $LiBa_{1-x}Gd_xPO_4$ compound, (x = 0, 0.04, 0.08), are presented in Fig. 4. Table 2 displays the precise positioning of the frequency bands for each of the samples under investigation. The spectral analysis reveals the presence of distinct peaks corresponding to the internal LiO_4 mode. These peaks are observed at approximately 412, 453, and 475 cm^{-1}, indicating the characteristic vibrational frequencies associated with the LiO_4 species. [23]. The prominent spectral feature observed at a wavenumber of 583 cm^{-1} is unequivocally attributed to the bending vibrations exhibited by the phosphate ion (PO_4^{3-}). The observed spectral feature, exhibiting a wide and pronounced maximum at a wavenumber of 1013 cm^{-1}, is attributed to the asymmetric stretching vibration of the P–O bond in the PO_4^{3-} ion. [24]**.** The confirmation of the formation of $LiBa_{1-x}Gd_xPO_4$ is substantiated by the detection of the phosphate group and the metal oxide vibrational band. These findings further validate the outcomes derived from X-ray diffraction (XRD) analysis.

3.4. Optical properties

3.4.1. Ultraviolet-Visible spectroscopic properties

The determination of the optical band gap was carried out through the utilization of a Tauc plot, specifically by analyzing the relationship between the square of the absorption coefficient $(\alpha h\nu)^2$ and the photon energy ($h\nu$), as denoted by Equation 1. Fig. 5 displays the Tauc plots of LiBa1-xGdxPO4, (x= 0, 0.04, and 0.08). These plots provide valuable insights into the band gap characteristics of the respective compositions. The band gap values obtained from the Tauc plots are determined to be 3.06 eV, 2.93 eV, and 2.14 eV for x = 0, 0.04, and 0.08, respectively. The bandgap energy of oxides exhibits a pronounced sensitivity to both the composition and crystal size of the materials, primarily as a result of quantum confinement phenomena [25]**.** It has been observed that the bandgap energy exhibits a decreasing trend as the crystallite size is increased. The observed phenomenon can be ascribed to the manifestation of the weak quantum confinement effect [26]**.** In accordance with the acquired findings, Fig. 6 presents a schematic depiction of the band structure.

$$\alpha h\nu = A\left(h\nu - E_g\right)^n \quad (1)$$

Where A is constant depends on transition type, which is given by n for direct bandgap n=1/2 (for indirect and forbidden transitions n=2, 3/2 respectively) as in our case, α is absorption coefficient, hν is energy of photon, E_g is energy bandgap and is calculated by plotting graph hν vs $(\alpha h\nu)^2$, tangent to these curves touching x-axis gives the band gap value.

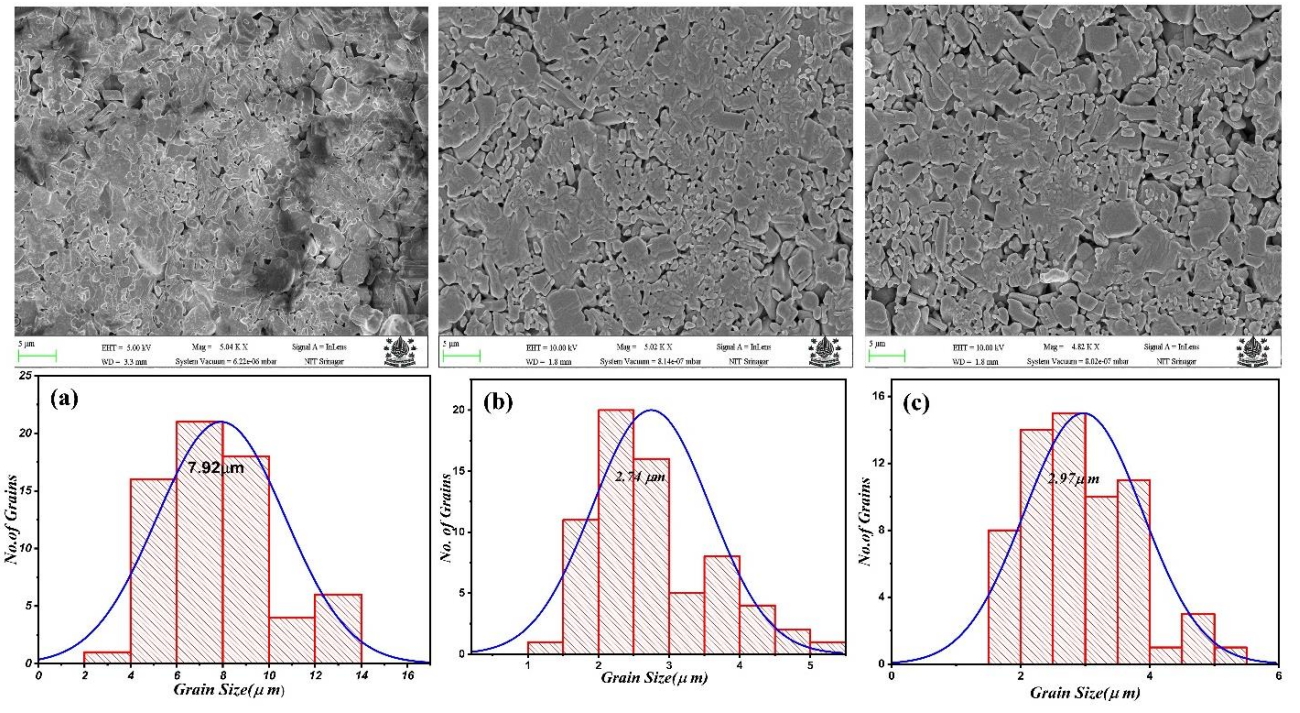

Fig. 3. FESEM images and corresponding Histograms of $LiBa_{(1-x)}Gd_xPO_4$; X= 0, 0.04, and 0.08.

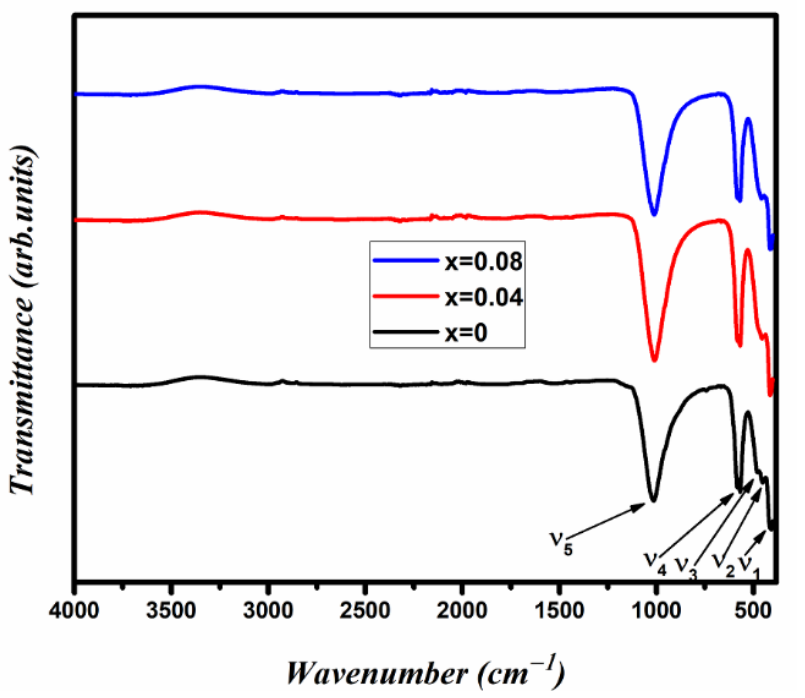

Fig. 4. FTIR spectra of $LiBa_{(1-x)}Gd_xPO_4$; X= 0.00, 0.04, and 0.08.

Table 2. Frequency bands of $LiBa_{1-x}Gd_xPO_4$ (x= 0, 0.04, and 0.08)

x	ν_1	ν_2	ν_3	ν_4	ν_5
0	412	453	476	583	1013
0.04	413	455	478	583	1013
0.08	413	459	475	583	1013

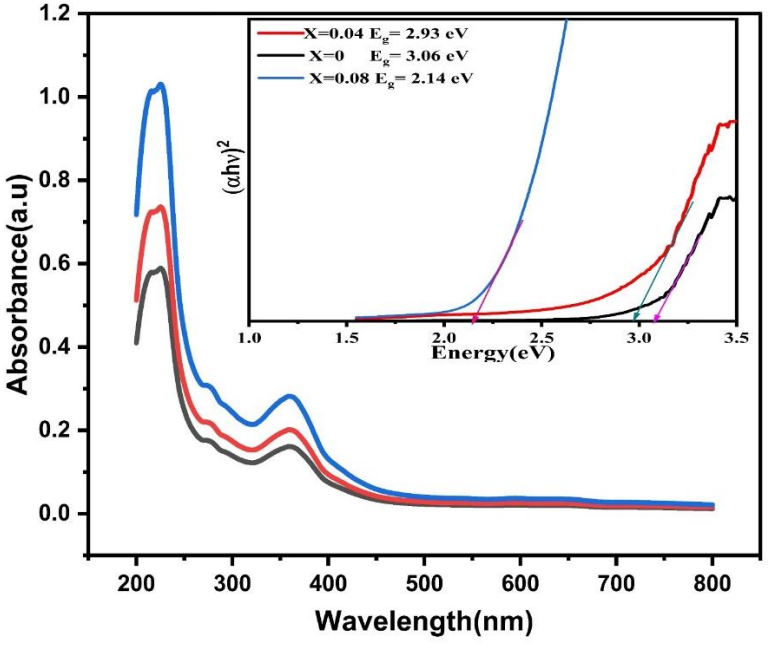

Fig. 5: Absorbance Spectra and Tauc Plots of $LiBa_{1-x}Gd_xPO_4$ (x= 0, 0.04, and 0.08).

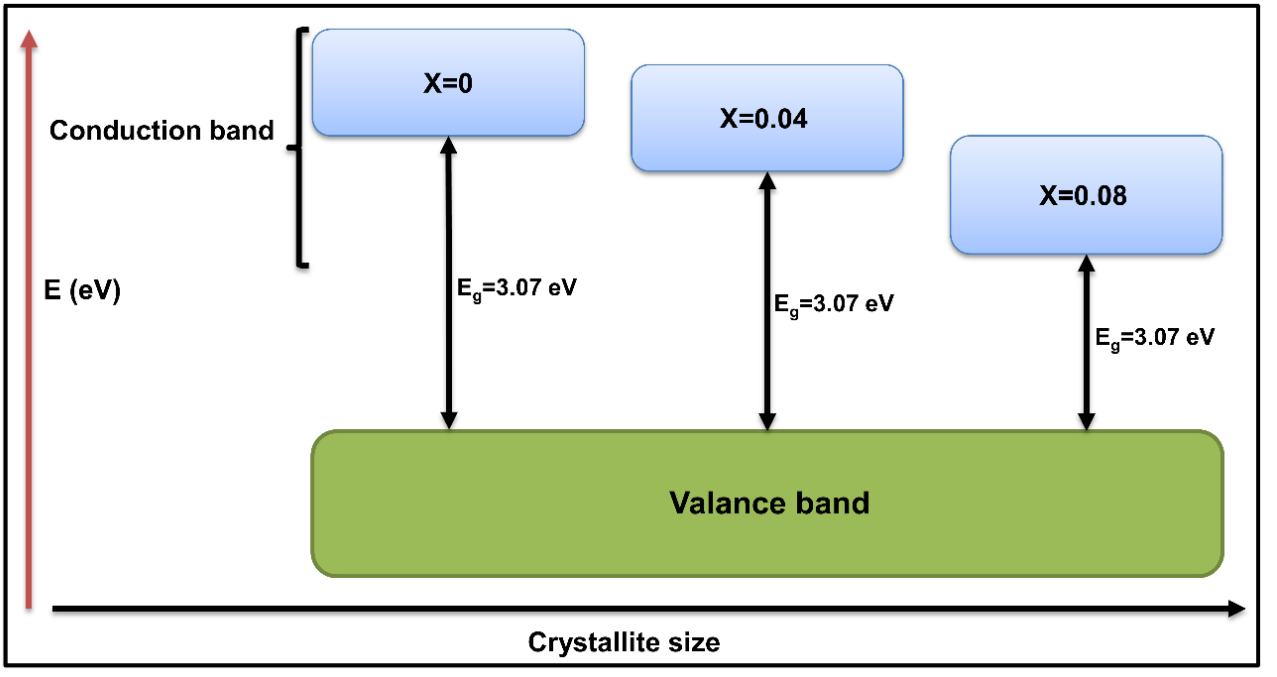

Fig. 6. Schematic representation of band-structure.

3.4.2. Photoluminescence properties

The utilization of photoluminescence spectra has been proposed as a viable method for ascertaining the valence state of Gd^{3+} ions. The photoluminescence exhibited by Gd^{+3} ions is characterized by its distinctiveness, primarily attributed to the f-f transitions occurring within the system. The determination of the precise positions, fine structure, and relative intensities of the bands in question is contingent upon the immediate surroundings of Gd^{3+}.

The photoluminescence (PL) spectra of $LiBa_{1-x}Gd_xPO_4$, where x takes on the values of 0, 0.04, and 0.08, were observed and recorded at room temperature. The emission wavelength used for the measurements was 624 nm. The obtained PL spectra are depicted in Fig. 7. In the present study, the investigation of phosphorous $LiBa_{1-x}Gd_xPO_4$ (where x represents the varying concentrations of Gd dopant) has yielded noteworthy findings. Specifically, the main spectral features of interest have been observed at distinct wavelengths. These sharp bands, which exhibit characteristic absorption behavior, have been identified at 253 nm, 274 nm, and 311 nm. The aforementioned wavelengths correspond to the respective concentrations of Gd dopant, namely x = 0, 0.04, and 0.08. These observations provide valuable insights into the optical properties of the phosphorous $LiBa_{1-x}Gd_xPO_4$ system, shedding light on the behavior of the material under investigation. The observed phenomenon of the electric dipole transition from the $^5D_0$ state to the $^7F_0$ state can be attributed to the primary peak, which is prominently located at a wavelength of 311 nm. The observed spectral peaks, with their respective centers at 253 and 274 nm, can be attributed to the magnetic dipole transition from the $^5D_0$ state to the $^7F_1$ state. The dominance of the electronic dipole transition arises due to the occupation of low symmetry by Gd^{3+} ions. In the present investigation, a notable augmentation in the intensity of photoluminescence (PL) spectra is observed, followed by a subsequent decline. The observed reduction in intensity may be attributed to the non-radiative energy transfer occurring between the Gd^{3+} ions, likely resulting from multipole-multipole interactions. According to Dexter's theory, the multipole-multipole interactions exhibit a distance-dependent behavior. [27, 28]. It was observed that as the concentration of Gd^{3+} ions was systematically increased, a notable phenomenon emerged. Specifically, an intriguing non-radiative pathway manifested, which could be attributed to the occurrence of energy transfer among the Gd^{3+} ions. This finding suggests the presence of an intricate interplay between the concentration of Gd^{3+} ions and the energy transfer dynamics within the system. Further investigation is warranted to comprehensively understand the underlying mechanisms governing this intriguing phenomenon. The observed phenomenon can be attributed to the reduced interionic separation between the Gd^{3+} ions. The determination of the critical distance between Gd^{3+} ions, arising from the phenomenon of energy transfer, can be computed utilizing the methodology proposed in the literature [29]. $R_c = 2[3V/4\Pi x_c z]^{1/3}$, where the volume of the unit cell is V, the critical concentration of the activator ion is x_c and Z is the number of formula units per unit cell. In the case of $LiBaPO_4$ Z=4, x_c =0.04 and V= 196.4145, hence the value of R_c =1.95nm which is 19Å. Because R_c is greater than 5 Å exchange contact is not responsible for non-radiative energy transfer between various Gd^{+3} ions in the host. The elevated magnitude of R_c can be ascribed to the inherent rigidity of the host matrix, which arises from the presence of a phosphate tetrahedral network. Additionally, the overlapping of the absorption and emission bands contributes

to the observed high value of R_c. The quenching mechanism can be attributed to the exchange interaction. In the realm of molecular interactions, various types of intermolecular forces manifest, namely dipole-dipole (d-d), dipole-quadrupole (d-q), and quadrupole-quadrupole (q-q) interactions. The experimental findings unequivocally demonstrate that the optimal concentration for achieving desirable outcomes in the $LiBa_{1-x}Gd_xPO_4$ system is precisely 0.01. Remarkably, it can be confidently asserted that the introduction of this specific doping concentration leads to the manifestation of a vivid red emission [30].

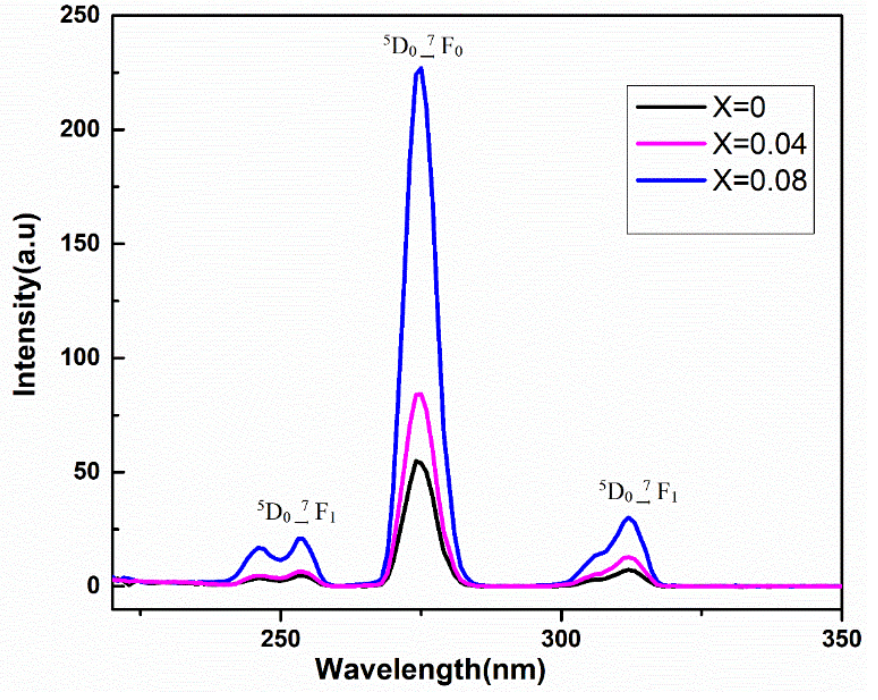

Fig. 7. Photoluminescence spectra of pristine and Gd-doped $LiBaPO_4$.

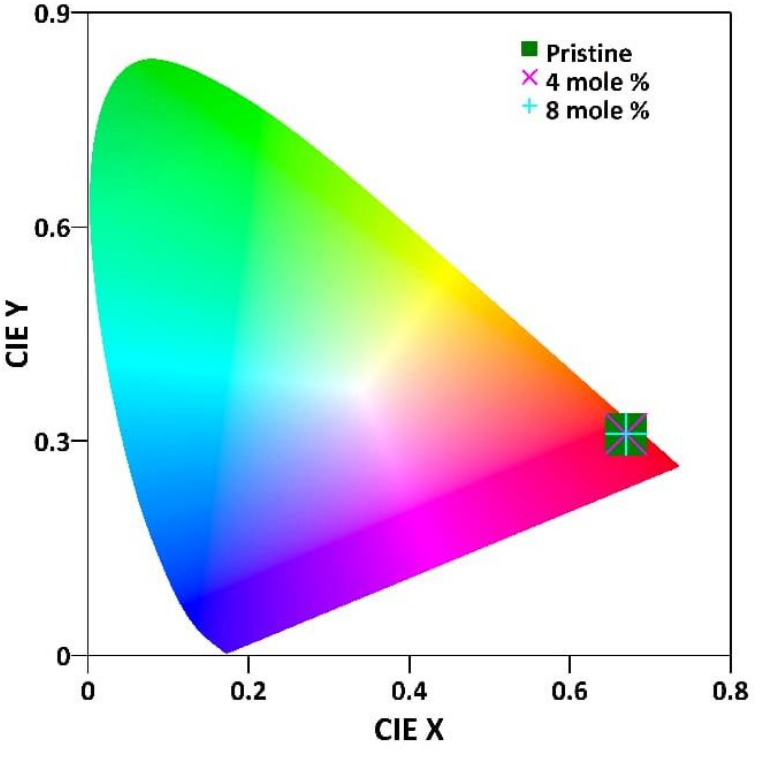

Fig. 8. CIE chromaticity diagram of $LiBa_{1-x}Gd_xPO4$ (x= 0, 0.04, and 0.08)

Table 3. CIE chromaticity coordinates of $LiBa_{1-x}Gd_xPO_4$ (x= 0, 0.04, and 0.08)

Conc.X	x	y	Color purity%
0.00	0.6691	0.3102	93.8
0.04	0.6794	0.3049	95.3
0.08	0.6736	0.3095	95

Chromaticity diagram for Gd doped $LaBaPO_4$ phosphor spheres is assessed from the emission spectra and the Commission International de I'Echairage (CIE) 1931 and are determined to be (0.6691, 0.3102) , (0.6794, 0.3049) and (0.6736, 0.3095) as depicted in Fig. 8 and Table 3. The addition of Gd^{3+} ions result in slight increase in x-coordinates and a small decrease in y-coordinate, which has been detected from the CIE coordinates. This strongly confirms the brilliant red color index [31]**.** The color purity was found to be above 90% in all the three samples and was found to be maximum in (0.04) doping of Gd^{3+} in $LaBaPO_4$ (95.3%).The expression for color purity is given as [32]:

$$Color\ \ purity = \sqrt{\frac{(x-x_i)^2+\ (y-y_i)^2}{(x_d-x_i)^2+(y_d-y_i)^2}} \times 100\% \qquad (2)$$

whereas dominant wavelength coordinates (x_d , y_d) relative to CIE 1931.

4. CONCLUSION

In conclusion, our study investigated the impact of Gd^{3+} doping on the structural and optical properties of $LiBaPO_4$. The results provide insightful information regarding the modifications brought about by Gd^{3+} doping in this substance. The prospective uses of Gd^{3+}-doped $LiBaPO_4$ in numerous domains call for further investigation. The experiment's findings show that there is a direct link between the amount of doping present and the growth in crystallite size. The size of the crystallite significantly increased from 43 nm to 65 nm when the doping concentration increases from x=0 to x=0.08. Finally, it can be said that the samples that were seen showed crystallization in the trigonal phase with a P31c space group. $LiBaPO_4$ samples Fourier Transform Infrared (FTIR) spectra analysis clearly demonstrates the existence of distinctive peaks, providing compelling proof that the samples' trigonal phase was formed. Using the tauc plot technique, the band gaps of the samples were calculated, and the results were 3.07 eV, 3.00 eV, and 2.27 eV, respectively. The bandgap energy decreases with increasing crystallite size. This finding offers important new understanding of how bandgap energy behaves in our particular scenario in respect to crystallite size, the weak quantum confinement effect may be used to explain the observed result. According to the photoluminescence results, it can be concluded that the bright red luminescent phosphor spheres are a good choice for use in red luminescent optical devices since they exhibit the requisite qualities.

CONFLICT OF INTEREST

The authors declare that there is no conflict of interests.

ACKNOWLEDGEMENTS

The authors gratefully acknowledge the Central Research Facility Center (CRFC) of the National Institute of Technology (NIT), Srinagar, India, for providing instrumentation facilities, including P-XRD, FESEM, and EDAX. We also extend our gratitude to the Chemistry Department at NIT Srinagar, India, for providing FTIR and UV-DRS characterization facilities. Additionally, we acknowledge the Nanotechnology Department of the University of Kashmir, India, for providing the PL facility. Showkat Ahmad Bhat, one of the authors, is particularly appreciative of the financial support from the Ministry of Human Resource Development (MHRD).

REFERENCES

[1] Li, M., Qiu, J., Ming, H., Zhao, P., Jin, Z., Zhang, S. and Yang, Y., **2019.** A SiO_x/Sn/C hybrid anode for lithium-ion batteries with high volumetric capacity and long cyclability. *Journal of Alloys and Compounds*, *809*, p.151659.

[2] Qu, M., Li, H., Zhao, Y. and Zhang, X.M., **2019.** Single-Component Color-Tunable Gd $(pic)_3$: Eu^{3+} Phosphor Based on a Metal–Organic Framework for Near-UV White-Light-Emitting Diodes. *ACS Omega*, *4*(2), pp.3593-3600.

[3] Kaur, H. and Jayasimhadri, M., **2020.** Optimization of structural and luminescent properties with intense red emitting thermally stable Sm^{3+} doped $CaBiVO_5$ phosphors for w-LED applications. *Optical Materials*, *107*, p.110119.

[4] Annadurai, G., Devakumar, B., Guo, H., Vijayakumar, R., Li, B., Sun, L., Huang, X., Wang, K. and Sun, X.W., **2018.** Novel Eu^{3+}-activated $Ba_2Y_5B_5O_{17}$ red-emitting phosphors for white LEDs: high color purity, high quantum efficiency and excellent thermal stability. *RSC Advances*, *8*(41), pp.23323-23331.

[5] Zhu, H., Fang, M., Huang, Z., Liu, Y.G., Chen, K., Min, X., Mao, Y. and Wang, M., **2016**. Photoluminescence properties of $Li_2Mg_2(WO_4)_3$: Eu^{3+} red phosphor with high color purity for white LEDs applications. *Journal of Luminescence*, *172*, pp.180-184.

[6] Elammari, L., Elouadi, B. and Müller-Vogt, G., **1988**. Study of phase transitions in the system $A_1B_{11}PO_4$ with A1= Li, Rb and B11= Mg, Ca, Sr, Ba, Zn, Cd, Pb. *Phase Transitions*, *13*(1-4), pp.29-32.

[7] Gao, G., Turshatov, A., Howard, I.A., Busko, D., Joseph, R., Hudry, D. and Richards, B.S., **2017**. Up-conversion fluorescent labels for plastic recycling: a review. *Advanced Sustainable Systems*, *1*(5), p.1600033.

[8] Hamrita, A., Slimani, Y., Salem, M.B., Hannachi, E., Bessais, L., Azzouz, F.B. and Salem, M.B., **2014**. Superconducting properties of polycrystalline $YBa_2Cu_3O_7$–d prepared by sintering of ball-milled precursor powder. *Ceramics International*, *40*(1), pp.1461-1470.

[9] Seevakan, K., Manikandan, A., Devendran, P., Slimani, Y., Baykal, A. and Alagesan, T., **2019**. Structural, magnetic and electrochemical characterizations of $Bi_2Mo_2O_9$ nanoparticle for supercapacitor application. *Journal of Magnetism and Magnetic Materials*, *486*, p.165254.

[10] Slimani, Y., Selmi, A., Hannachi, E., Almessiere, M.A., Mumtaz, M., Baykal, A. and Ercan, I., **2019**. Study of tungsten oxide effect on the performance of $BaTiO_3$ ceramics. *Journal of Materials Science: Materials in Electronics*, *30*, pp.13509-13518.

[11] Slimani, Y., Almessiere, M.A., Shirsath, S.E., Hannachi, E., Yasin, G., Baykal, A., Ozcelik, B. and Ercan, I., **2020**. Investigation of structural, morphological, optical, magnetic and dielectric properties of (1-x) $BaTiO_3$/x$Sr_{0.92}Ca_{0.04}Mg_{0.04}Fe_{12}O_{19}$ composites. *Journal of Magnetism and Magnetic Materials*, *510*, p.166933.

[12] Slimani, Y., Unal, B., Hannachi, E., Selmi, A., Almessiere, M.A., Nawaz, M., Baykal, A., Ercan, I. and Yildiz, M., **2019**. Frequency and dc bias voltage dependent dielectric properties and electrical conductivity of $BaTiO_3SrTiO_3$/(SiO_2)x nanocomposites. *Ceramics International*, *45*(9), pp.11989-12000.

[13] Anastasiou, E., Lorentz, K.O., Stein, G.J. and Mitchell, P.D., **2014**. Prehistoric schistosomiasis parasite found in the Middle East. *The Lancet Infectious Diseases*, *14*(7), pp.553-554.

[14] Peng, Y.M., Su, Y.K. and Yang, R.Y., **2013**. The charge transfer transition phenomenon and microstructure of Eu^{3+}-doped $NaCaPO_4$ phosphors sintered with NH_4Cl flux via solid-state reaction. *Materials Research Bulletin*, *48*(5), pp.1946-1951.

[15] Yang, R.Y., Peng, Y.M. and Su, Y.K., **2013**. Novel red-emitting microwave-assisted-sintered $LiSrPO_4$: Eu^{3+} phosphors for application in near-UV white light-emitting diodes. *Journal of Electronic Materials*, *42*, pp.2910-2914.

[16] Zhang, S., Nakai, Y., Tsuboi, T., Huang, Y. and Seo, H.J., **2011**. Luminescence and microstructural features of Eu-activated $LiBaPO_4$ phosphor. *Chemistry of Materials*, *23*(5), pp.1216-1224.

[17] Zhang, S., Wei, D., Zhu, R., Huang, Y. and Seo, H.J., **2011**. The luminescence and structural characteristics of Eu^{3+}-doped $NaBaPO_4$ phosphor. *Ceramics International*, *37*(8), pp.3697-3702.

[18] Ramteke, S.K., Yerpude, A.N., Dhoble, S.J. and Kokode, N.S., **2020**. Luminescence characterization of $KBaPO_4$: RE (RE= Sm^{3+}, Eu^{3+}, Dy^{3+}) phosphors. *Luminescence*, *35*(6), pp.969-973.

[19] Acosta-Humánez, F., Almanza, O. and Vargas-Hernández, C., **2014**. Effect of sintering temperature on the structure and mean crystallite size of $Zn_{1-x}Co_xO$ (x= 0.01-0.05) samples. *Superficies Y Vacío*, *27*(2), pp.43-48.

[20] Lone, G.A. and Ikram, M., **2022**. Investigating the structural and dielectric properties of $CoFe_2-$ xNi_xO_4 spinel ferrite. *Journal of Alloys and Compounds*, *908*, p.164589.

[21] Cao, R., Quan, G., Shi, Z., Gou, Q., Chen, T., Hu, Z. and Luo, Z., **2018**. Synthesis and luminescence properties of $LiBaPO_4$: Bi^{3+} yellow-emitting phosphor for solid-state lighting. *Journal of Materials Science: Materials in Electronics*, *29*, pp.5287-5292.

[22] Dholabhai, P.P., Adams, J.B., Crozier, P. and Sharma, R., **2010**. A density functional study of defect migration in gadolinium doped ceria. *Physical Chemistry Chemical Physics*, *12*(28), pp.7904-7910.

[23] Kumar, I. and Gathania, A.K., **2022**. Photoluminescence and quenching study of the Sm^{3+}-doped $LiBaPO_4$ phosphor. *Journal of Materials Science: Materials in Electronics*, *33*(1), pp.328-341.

[24] Paques-Ledent, M.T., **1978**. Vibrational spectra and structure of $LiB^{2+}PO_4$ compounds with B= Sr, Ba, Pb. *Journal of Solid State Chemistry*, *23*(1-2), pp.147-154.

[25] Agú, U.A., Oliva, M.I., Marchetti, S.G., Heredia, A.C., Casuscelli, S.G. and Crivello, M.E., **2014**. Synthesis

and characterization of a mixture of $CoFe_2O_4$ and $MgFe_2O_4$ from layered double hydroxides: Band gap energy and magnetic responses. *Journal of Magnetism and Magnetic Materials*, *369*, pp.249-259.

[26] Massoudi, J., Smari, M., Nouri, K., Dhahri, E., Khirouni, K., Bertaina, S. and Bessais, L., **2020**. Magnetic and spectroscopic properties of Ni–Zn–Al ferrite spinel: from the nanoscale to microscale. *RSC Advances*, *10*(57), pp.34556-34580.

[27] Dexter, D.L., **1953**. A theory of sensitized luminescence in solids. *The Journal of Chemical Physics*, *21*(5), pp.836-850.

[28] Liu, X., Lin, C. and Lin, J., **2007**. White light emission from Eu3+ in CaIn2O4 host lattices. *Applied Physics Letters*, *90*(8).

[29] Lucas, F., Jaulmes, S., Quarton, M., Le Mercier, T., Guillen, F. and Fouassier, C., **2000**. Crystal structure of $SrAl_2B_2O_7$ and Eu^{2+} luminescence. *Journal of Solid State Chemistry*, *150*(2), pp.404-409.

[30] Irvine, J.T.S., **1990.** New compounds and structures. *Annual Reports Section" A"(Inorganic Chemistry)*, *87*, pp.181-197.

[31] Kumar, K.N., Vijayalakshmi, L. and Kim, J.S., **2018**. Enhanced red luminescence quantum yield from Gd^{3+}/Eu^{3+}: $CaLa_2ZnO_5$ phosphor spheres for photonic applications. *Materials Research Bulletin*, *103*, pp.234-241.

[32] Singh, V., Lakshminarayana, G. and Wagh, A., **2020**. Photoluminescence investigation on green-emitting Tb^{3+}-doped $BaLa_2ZnO_5$ nanophosphors. *Journal of Electronic Materials*, *49*, pp.510-517.